High-throughput metal nanoparticle catalysis by pulsed laser ablation

Michael Kahn, Selim Senkan

Abstract

A high-throughput pulsed laser ablation (HT-PLA) system was developed to rapidly prepare uniformly sized single- and multi-metallic nanoparticles with different diameters for catalytic applications. Catalytic materials containing Rh, bimetallic Rh/Pt and trimetallic Rh/Pt/Au nanoparticles were synthesized from targets prepared by blending, tableting and sintering powders of pure metals, and by directly collecting the nanoparticles created on support materials. Nanoparticles exhibited crystallinity and uniformity in size and composition as determined by high resolution transmission electron microscopy (HR-TEM) and energy dispersive X-ray (EDX) spectroscopy, respectively. The supported nanoparticles created by HT-PLA were also screened for their catalytic activities and selectivities for the partial oxidation of propylene. In less than a day, over 40 different catalytic materials of nanoparticles supported on Al_2O_3, CeO_2, TiO_2, SiO_2 and Y-ZrO_2 were prepared and evaluated. This highly streamlined approach resulted in the discovery of TiO_2 supported 0.004 wt% Rh nanoparticles as a promising new lead for the synthesis of partial oxidation products of propylene with one-pass yields of about 13% at 275C.

Introduction

Pulsed laser ablation (PLA) represents a highly versatile and powerful approach for the preparation of uniformly sized multi-metallic nanoparticles for catalytic applications. Laser ablation is a phenomenon in which material is ejected froma solid surface as a consequence of rapid energy deposition by light irradiation [10]. Rapid energy deposition results in surface heating and ionization leading to coulombic and thermal explosion concomitant with the formation of high temperature (i.e. plasma) gas and shock waves. PLA is already being exploited in a number of technological applications such as small device fabrication, pulsed laser deposition (PLD) of thin films and coatings [11], laser surgery [12] and matrix assisted laser desorption ionization (MALDI) [13].

PLA is suitable for the synthesis of catalytic metallic nanoparticles for a number of reasons. First, virtually any metal or mixtures in any composition and form, e.g. sheet, film, powder, can be transformed into nanoparticles with a reasonably narrow size distribution using high power pulsed lasers [10]. Consequently, PLA avoids the use of dangerous or expensive liquid or gaseous precursor chemicals. Second, nanoparticles prepared by PLA can directly be collected on catalyst supports, thereby eliminating the need to handle potentially toxic nanopowders. Since nanoparticles can be created with a significant number of dangling bonds, because they originate from a high temperature plasma gas, they can be strongly adsorbed, thus become anchored on supports. This decreases their mobility and inhibits particle sintering during reactions. This is a distinct advantage of PLA compared to solution based methods that tend to passivate particle surfaces by moieties present in the reaction medium. Third, PLA creates no byproducts and can be scaled up for industrial applications. Finally, the sizes and the compositions of the nanoparticles generated by PLA can be adjusted to generate materials for specific catalytic and other applications.

Experimental

In Fig. 1, the HT-PLA system developed is shown. The setup consists of a rotatable target holder that houses multiple targets (24 cylindrical targets with 1.25 cm diameters in the current design). The target under laser illumination is continuously spun at a rate of about 5–10 rpm for the better utilization of the target material. A pulsed laser beam (Lambda Physik Compex 100 Excimer Laser, 300 mJ/pulse, 30 ns pulse duration) is focused to a spot of about 0.1 cm diameter, off axis on the surface of the target, arriving at an angle of about 45 degrees. Nanoparticles created in the ablation plume are then collected either on support pellets (0.4 cm diameter x 0.1 cm thick cylinders), on standard transmission electron microscope (TEM) grids, or single crystal silicon wafers as shown in Fig. 1-E. Consequently, it is possible to readily characterize the nanoparticles before reaction screening. In the current design, a rotatable holder is used to house up to 30 support pellets and/or TEM grids. A mask prevents cross contamination of the sites. The distance between the target and collection site can also be adjusted. This assembly is placed inside a gas tight (vacuum) chamber to control the ambient gas conditions during PLA (Ar in the present experiments). The laser beam is introduced into the chamber through a UV transparent fused silica window.

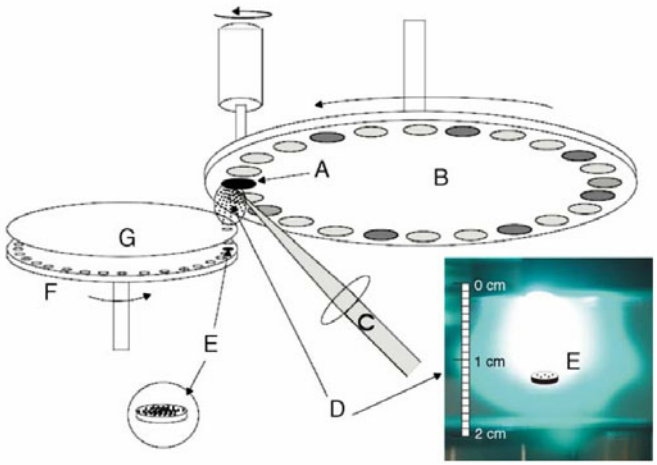

Fig. 1. A sketch of the high-throughput pulsed laser ablation (HT-PLA) system that enables the rapid preparation of a large number of supported multi-metallic nanoclusters: (A) ablating target, (B) rotatable (selectable) target holder, (C) pulsed laser beam, (D) ablation plume, (E) catalyst support or TEM grid containing nanoparticles, (F) catalyst support or TEM grid holder and (G) mask. All the components are placed in a gas tight (vacuum) chamber for the control of pressure and the nature of the ambient gas. A multitude of different targets (24 shown) can be ablated sequentially, and the nanoparticles created can be deposited directly on support pellets or TEM grids. The pellets can then be used for catalytic screening. A mask is used to prevent cross contamination of sites. The distance between the target and support pellets can also be adjusted. The pulsed laser beam enters the chamber through a fused silica window and irradiates the target at a 45 angle. The target under illumination is continuously spun at 5–10 rpm for the better utilization of the target material. Also shown is a rhodium metal ablation plume showing the target and schematic collection of nanoparticles on the external surface of support pellets, TEM grids or silicon wafers, by placing them inside the plume.

Results and Discussion

In Fig. 2, TEM pictures of Rh nanoparticles collected on carbon film are shown as function of distance along the ablation plume, together with their corresponding number statistics and number densities (see Fig. 1, inset for a spatial reference). Fig. 3 clearly shows a narrow and adjustable particle size distribution, with particle diameters decreasing with distance from the target. Mean particle diameters were about 6, 3 and 1 nm, at 1.3, 1.6 and 1.9 cm from the target, respectively. It is interesting to note that the particle size distributions also become narrower with increasing distance from the target.

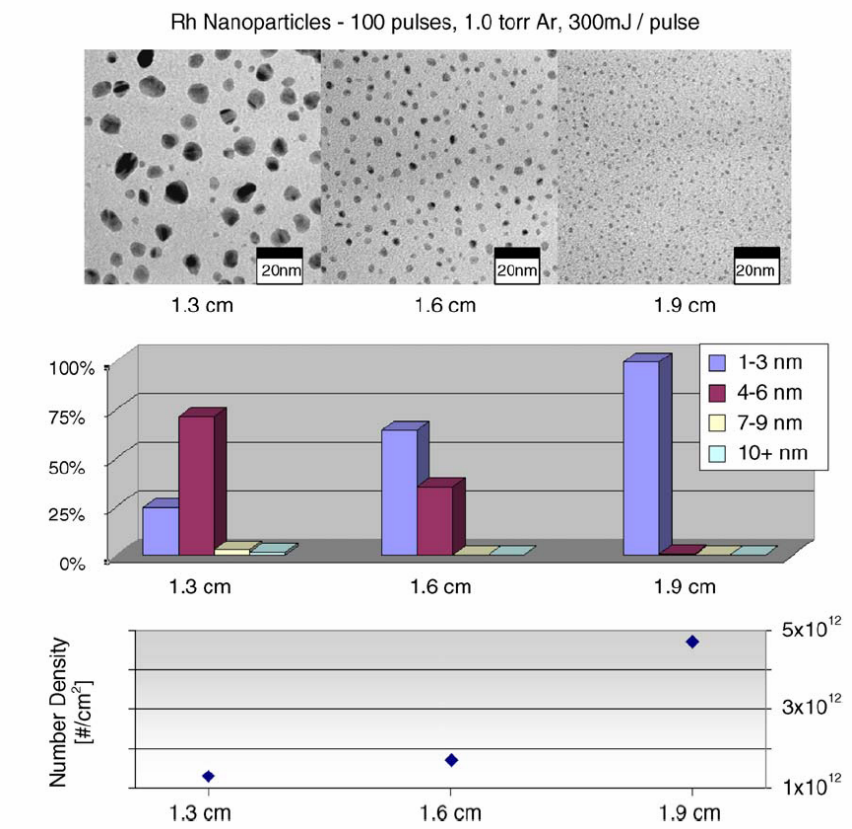

Fig. 2. Rhodium metal nanoparticles collected on carbon film at 1.3, 1.6 and 1.9 cm along the ablation plume (see Fig. 1 for spatial reference). Ablation conditions were the following: 100 pulses, 248 nm KrF excimer laser operating at 300 mJ/pulse and 30 ns pulse width, 1 Torr Ar ambient pressure. On top are the TEM images (JEOL JEM-2000FX), which clearly show that particle diameters decrease with increasing distance from the target. The black line inserts correspond to 20 nm scale. Particle number statistics shown in the middle figure clearly support this trend. For example, the fractions of smaller particles (1–3 nm) increase, while those for 4–6 nm and larger decrease with distance along the ablation plume. In contrast, the number densities of particles steadily increase along the plume, consistent with the fragmentation of energetic larger particles into smaller ones and/or nucleation and growth of new particles.

In Fig. 3, the high-resolution TEM (HR-TEM) images of bimetallic Rh/Pt and trimetallic Rh/Pt/Au nanoparticles created by the HT-PLA system are shown, together with representative EDX spectra. These particles were created from tablets prepared by blending and pressing 325 mesh 99.9% pure metal powders at approximate weight ratios of 50/50 and 40/40/20 for the Rh/Pt and Rh/Pt/Au cases, respectively, followed by sintering at 700C for 20 min under Ar gas.

The images in Fig. 3 correspond to nanoparticles collected at about 2 cm from the target for 100 pulses, while keeping all other variables constant. As evident from this figure, the particles were crystalline and uniformly sized with diameters in the range of 1–3 nm.

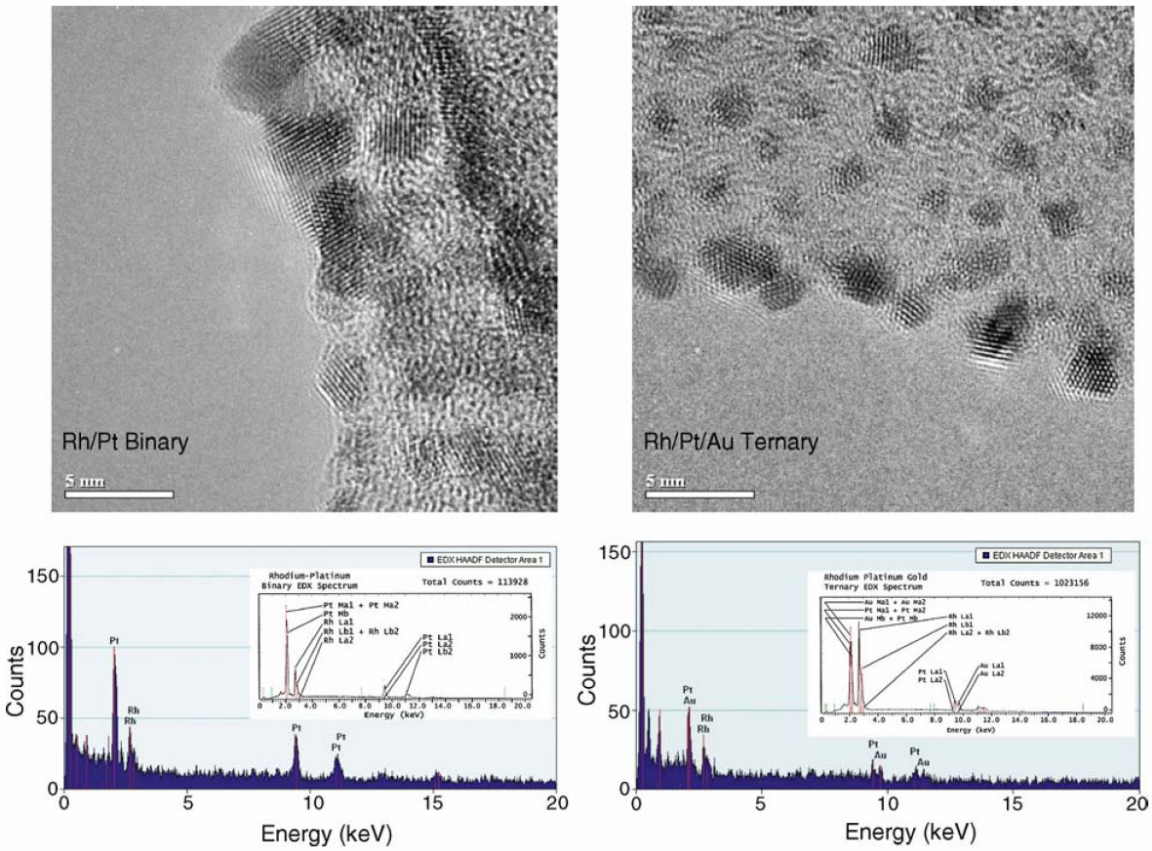

Fig. 3. High-resolution transmission electron microscope (HR-TEM) images of bimetallic Rh/Pt (left) and trimetallic Rh/Pt/Au (right) nanoparticles created by HT-PLA and determined by high-resolution TEM (FEI Tecnai TF30UT, 300 kV HT, FEG source with ultra twin lens) and the corresponding representative energy dispersive X-ray (EDX) spectra of individual particles, where Cu peaks corresponding to the TEM grid were removed for clarity. The EDX spectra of the targets, determined separately using a SEM (Cambridge Stereoscan 250) are also presented as inserts. The similarity of EDX spectra suggests that the compositions of the nanoparticles formed are similar to those of the corresponding target materials. As evident from these pictures, nanoparticles were crystalline, with particle diameters in the 1–3 nm range. The EDX spectra also indicate the presence of all the constituent metals within the nanoparticles. The EDX analysis of several distinct particles also exhibited similar spectra, indicating the compositional similarity of different nanoparticles.

Next, the HT-PLA was integrated with array channel microreactors and mass spectrometry (MS) [14] for the catalytic evaluation of supported metal nanoparticles for the industrially important reaction of propylene partial oxidation. For this, we prepared over 40 different catalytic materials consisting of nanoparticles of Rh, binary Rh/Pt and ternary Rh/Pt/Au supported on porous pellets of Al_2O_3 (BET surface area 128 m^2/g), CeO_2 (17 m^2/g), TiO_2 (268 m^2/g), SiO_2 (325 m^2/g) and Y-ZrO_2 (37 m^2/g) at about 2 cm in the ablation plume. Different metal loadings were achieved by using 1, 10, 100 and 1000 laser pulses. The preparation of these 40 catalytic materials took approximately 3 h.

Catalyst evaluation was performed under atmospheric pressure and at temperatures of 250, 275 and 300C using a feed stream of 20% propylene (PR) and C_3H_6/O_2 ratios of 0.25, 0.5, 1, 2 and 4, with the balance being helium. The gas hourly space velocity (GHSV) was 20,000

h^{-1}. The partial oxidation of propylene can form a variety of products such as propylene oxide (PO), acetone (AT), acrolein (AC) and propanal (PaL) [15]. In Fig. 4, selected results from these screening experiments are presented in a multi-dimensional matrix format. As defined in the figure caption, larger spots correspond to higher PO + AC yields (mass 58), thus are desirable. As can be seen in Fig. 4, supported single Rh nanoparticles were the best performers among all the different catalytic materials evaluated, and these results are presented in the first column. In particular, TiO_2 supported Rh nanoparticles at 100 pulse loading led to the highest yield (Y_{PO+AT}) of 13% at 275C in our experiments, which is also indicated in the legend.

In summary, the HT-PLA has been shown to be a versatile technique for the rapid creation of multi-metallic nanoparticles that are crystalline and uniform in size and composition, from readily available powders of pure metals. Since the amount of metals used in the creation of nanoparticle catalysts is small, HT-PLA can readily be scaled up to have an impact on industrial heterogeneous catalysis. The HT-PLA, in conjunction with high-throughput catalyst screening methods, has also been shown to significantly increase the tempo of research for the discovery and optimization of supported nanoparticle catalysts, as demonstrated by the discovery of new leads for the propylene partial oxidation reactions.

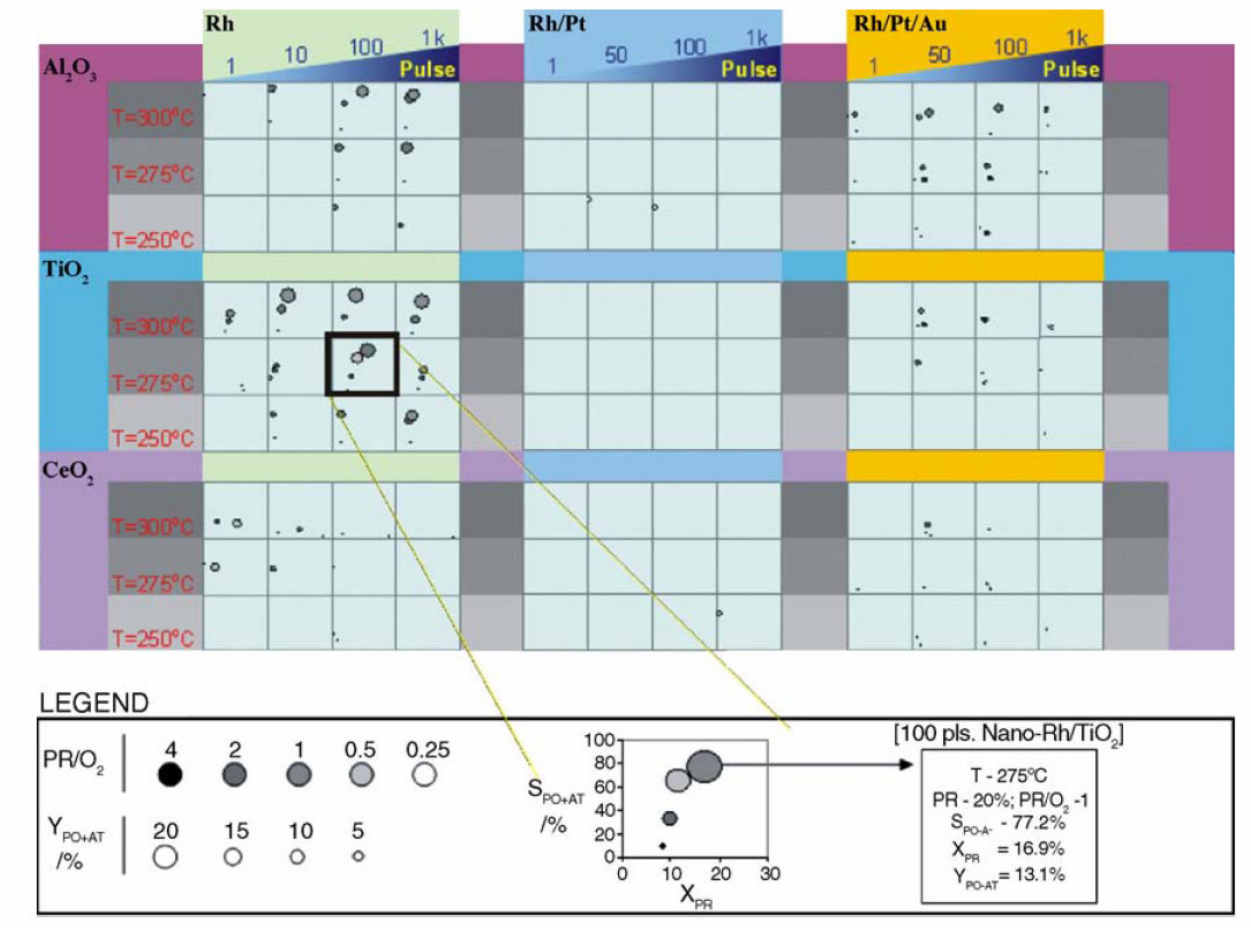

Fig. 4. Selected results for mass 58 production, i.e. propylene oxide (PO) + acetone (AT), on Al_2O_3, TiO_2 and CeO_2 supported nanoparticles of Rh, binary Rh/Pt and ternary Rh/Pt/Au displayed in a multi-dimensional matrix format. In each square, mass 58 selectivity (S_{PO+AT}) vs. propylene (PR) conversion (XPR) is plotted for one catalyst, with PO + AT yields ($Y_{PO+AT} = S_{PO+AT} * X_{PR}$) presented by the sizes of the circles or spots (see legend). Different circles

in each square correspond to different C_2H_6/O_2 ratios used in the experiments, in accordance with the gray scale shown in the legend. Within each group, columns from left to right correspond to increased nanoparticle loadings, corresponding to increased number of laser pulses (1, 10, 100 and 1000 pulses). Different rows correspond to different reaction temperatures (250, 275 and 300C) for each support material as indicated. The pressure was atmospheric with GHSV of 20,000 h^{-1}. Among all the catalytic materials considered, TiO_2 supported 100 pulse Rh was the best performer producing PO + AT at a yield of 13% at 275C, details of which are shown in the legend section. Multi-metallic materials exhibited poor PO + AT yields because of excessive combustion by Pt. The presence of optimal nanoparticle loading is evident for single Rh loading on TiO_2 at 300C. The decrease in selectivity and yield at high laser pulses is likely due to increased particle overlap thus film formation.

References

[1] National Institute of Standards and Technology, Advanced Technology Program, Catalysis and Biocatalysis, White Paper, 1998

M.E. Davis, Future directions in catalysis: structures that function at the nanoscale, in: NSF Workshop, June 19–20, 2003;

J.M. White, Opportunities for catalysis in the 21st century, in: Basic Energy Sciences Advisory Committee Subpanel Workshop, Department of Energy, May 14–16, 2002.

[2] National Research Council, Catalysis Looks to the Future, National Academy Press, Washington, DC, 1992.

[3] G. Poncelet, J. Martens, B. Delmon, P.A. Jacobs, P. Grange (Eds.), Preparation of Catalysts VI, Elsevier, Amsterdam, The Netherlands, 1995.

[4] O.S. Alexeev, B.C. Gates, Ind. Eng. Chem. Res. 42 (2003) 1571.

[5] T. Hayashi, K. Tanaka, M. Haruta, J. Catal. 178 (1998) 566.

[6] M. Valden, X. Lai, D.W. Goodman, Science 281 (1998) 1647.

[7] J.D. Aiken, R.G. Finke, J. Mol. Catal. A. Chem. 145 (1999) 1.

[8] M.T. Swinehart, Curr. Opin. Colloid Interface Sci. 8 (2003) 127.

[9] A. Avoyan, G. Rupprechter, A.S. Eppler, G.A. Somorjai, Top. Catal. 10 (2000) 107.

[10] W. Marine, L. Patrone, B. Luk'yanchuk, M. Sentis, Appl. Surf. Sci. 154–155 (2000) 345; L.V. Zhigilei, Appl. Phys. A76 (2003) 339.

[11] M.N.R. Ashfold, F. Claeyssens, G.M. Fuge, S.J. Henley, Chem. Soc. Rev. 33 (2004) 23.

[12] E.L. Tanzi, J.R. Lupton, T.S. Alster, J. Am. Acad. Dermatol. 49 (2003) 1; S.C. Gibson, D.S. Bryne, A.J. McKay, Br. J. Surg. 91 (2004) 893.

[13] G. Corana, G. Toffoli, Comb. Chem. High Throughput Screen 7 (2004) 707.

[14] S. Senkan, Angew. Chem. Int. Ed. 40 (2001) 312; S.M. Senkan, S. Ozturk, Angew. Chem. Int. Ed. 38 (1999) 791; S.M. Senkan, K. Krantz, S. Ozturk, V. Zengin, I. Onal, Angew. Chem. Int. Ed. 38 (1999) 2794.

[15] T. Miyazaki, S. Ozturk, I. Onal, S. Senkan, Catal. Today 81 (2003) 473.